Comparison of Ion Coupling Strategies for a Microengineered Quadrupole Mass Filter

Steven Wright,[a] Richard R. A. Syms,[b] Shane O'Prey,[a] Guodong Hong,[a] and Andrew S. Holmes[b]

[a] Microsaic Systems Ltd., Woking, Surrey, United Kingdom
[b] Department of Electrical and Electronic Engineering, Imperial College, London, United Kingdom

The limitations of conventional machining and assembly techniques require that designs for quadrupole mass analyzers with rod diameters less than a millimeter are not merely scale versions of larger instruments. We show how silicon planar processing techniques and microelectromechanical systems (MEMS) design concepts can be used to incorporate complex features into the construction of a miniature quadrupole mass filter chip that could not easily be achieved using other microengineering approaches. Three designs for the entrance and exit to the filter consistent with the chosen materials and techniques have been evaluated. The differences between these seemingly similar structures have a significant effect on the performance. Although one of the designs results in severe attenuation of transmission with increasing mass, the other two can be scanned to $m/z = 400$ without any corruption of the mass spectrum. At $m/z = 219$, the variation in the transmission of the three designs was found to be approximately four orders of magnitude. A maximum resolution of $M/\Delta M = 87$ at 10% peak height has been achieved at $m/z = 219$ with a filter operated at 6 MHz and constructed using rods measuring (508 ± 5) μm in diameter. (J Am Soc Mass Spectrom 2009, 20, 146–156) © 2009 Published by Elsevier Inc. on behalf of American Society for Mass Spectrometry

Interest in the miniaturization of mass analyzers has been growing rapidly in recent years, largely driven by the need for compact, lightweight systems for use in environmental, security, and space applications. While there have been numerous attempts to make small analyzers, not all can reasonably be called miniature [1]. However, quadrupole mass filters [2–6] and various types of ion traps [7–9] with characteristic dimensions of the order of a few millimeters or less have been demonstrated. The size and weight contribution to a complete mass spectrometer system is not the only benefit of a miniaturized quadrupole mass filter. The rf amplitude required to achieve a particular mass range increases with the square of the rod radius. Hence, the rf supplies for miniature filters can be smaller and require less power than those needed for larger filters. More importantly, smaller pumps may be used, as the short path length of ions in the filter means that a higher pressure can be tolerated. Although this paper is focused on miniaturization of the filter, reports on the development of other miniaturized components that might be incorporated into a system, such as ion sources, gauges, and pumps can be found elsewhere [10–12].

The factors that determine the size of a miniature quadrupole mass filter are the required signal level, the accuracy of the construction technique, and the number of rf cycles needed to achieve the desired resolution. Clearly, as the size of the entrance aperture decreases, there will be an inevitable loss of signal, although some of this can be recovered through the use of an array [2, 4]. There is a well-known correlation [13] between the fractional geometrical error and ultimate resolution. Hence, one fundamental limitation is set by the accuracy of the fabrication technique and the minimum acceptable resolution. Similarly, it has been shown that the ultimate resolution increases with square of the number of rf cycles experienced by the ions in the filter [13]. The number of cycles, n, is given by $n = fL(m/2\text{eV})^{0.5}$, where f is the frequency, L is the length of the rods, m is the mass of the ion, and eV is the ion energy. Hence, the filter can be made smaller if the frequency and ion energy are adjusted to compensate for a reduced rod length. However, there are other factors that limit the extent to which this is feasible. Most importantly, the rf amplitude required to transmit a particular mass increases with the square of the frequency. Consequently, the size and design of the power supplies, heat dissipation in the filter, the minimum spacing required to avoid a discharge, and the desired mass range also need to be considered.

The resolution and mass range reported for miniature quadrupole filters, together with details of their size and operating parameters, are summarized in Table 1. There is substantial variation in the degree of miniaturization attempted and the level of performance

Address reprint requests to Professor R. R. A. Syms, Department of Electrical and Electronic Engineering, Imperial College, Exhibition Rd., South Kensington, London SW7 2AZ, UK. E-mail: r.syms@imperial.ac.uk

1044-0305/09/$32.00
doi:10.1016/j.jasms.2008.08.019

Published online September 5, 2008
Received March 17, 2008
Revised August 28, 2008
Accepted August 28, 2008

Table 1. Comparison of the mass range, resolution, construction details, and operating parameters reported for each of the miniature quadrupole mass filters. The reference in brackets indicates which peak width definition was used to calculate the resolution. The inscribed radius has been calculated assuming a rod ratio of 1.147

Group	Construction	Mass range (*m/z*)	M/ΔM	Inscribed radius (μm)	Rod length (mm)	Frequency (MHz)	Ion energy (eV)
JPL [2]	Machined ceramic jigs	300	600 (50%)	870	25	5.3–7.1	
Leybold Inficon [3]	Ceramic spacers	100	111 (10%)	330	12.5	13	
Ferran [4, 14]	Glass-to-metal seal	100	133 (50%)	870	10	14	5
MIT [5]	MEMS	650	99 (50%)	690	90	1.44	13.6
Liverpool/ICL [6]	MEMS	50	30 (10%)	217	20–30	6	2
Microsaic	MEMS	400	87 (10%) 200 (50%)	217	30	6	5–10

achieved. The inscribed radius (of a circle that can be drawn inside the four rods) is quoted rather than the rod radius, as one of the filters is constructed using hyperbolic electrodes. The peak width at either 50% or 10% peak height was used to calculate the resolution, as indicated by the figures in brackets. Typically, the resolution derived using the 10% definition is very approximately half the value derived using the 50% definition.

The overwhelming majority of commercially available quadrupole mass filters are constructed using rods with diameters in the range of 6 to 20 mm. An arrangement in which the rods are held tightly against an outer ceramic support collar using threaded studs or similar screwed into blind, tapped holes in the rods themselves has been widely adopted. This design has proven to be sufficiently rigid and tolerant of thermal expansion mismatch between materials. Techniques to fabricate the ceramic components have advanced to such a level that the alignment accuracy required for high-resolution can be readily achieved.

The construction of miniature quadrupole mass filters presents difficulties that are peculiar to microengineering and not generally encountered in the design of instruments of a more conventional size. Clearly, drilling and tapping holes in rods measuring less than 1 mm is likely to be very challenging. Hence, the most obvious difficulty is to devise a means of precisely supporting the rods in the correct geometry whilst also maintaining electrical isolation. Silicon-based microelectromechanical systems (MEMS) design approaches are ideally suited to the solution of these problems, as techniques for fabricating complex, multi-layer structures with micrometer precision are well-advanced. Quadrupoles [5, 6, 15–17] and traps [18, 19] have been constructed using MEMS technology, with varying degrees of success.

Apart from providing a means of supporting the rods, one of the other key challenges is the incorporation of components that allow the ions to be coupled into, and out of, the quadrupole field. For conventional instruments, there are essentially three different methods of successfully injecting ions. In residual gas analyzers and other low-end analyzers, it is usual to find a plate with an aperture at its center held directly in front of the rods. For best resolution, the size of the aperture should be chosen to select only ions that have initial trajectories close to the central axis of the quadrupole field. However, the initial trajectories of the ions are determined as much by the action of fringing fields as they are by the size of the input aperture. Fringing fields are known [13, 20, 21] to accelerate ions along the transverse y axis (which is conventionally taken as that for which the Mathieu a parameter is negative). This can result in trajectories that are unfavorable for optimum performance or even eject ions before they enter the rod assembly. In simple designs, the distance between plate and rod is minimized so as to reduce the time ions spend in the fringing fields. Applying a dc bias to all or part of the aperture plate is believed to alter the fringing fields in a way that reduces their effect [22]. In a second, somewhat more complex approach, the ions can be injected directly into the field between the rods through one or more biased conical lenses so that they bypass to a greater extent the problematic region at the very end of the rod assembly [23, 24]. In applications requiring high-resolution and sensitivity, particularly for higher mass ions, the use of a short, rf-only prefilter is the most common solution.

An early attempt [6] to make a miniature quadrupole filter using MEMS techniques was based on four cylindrical electrodes mounted in pairs on two oxidized silicon substrates that were held apart by two cylindrical spacers. The filter rods and the spacers were all accurately aligned and supported by the use of V-grooves etched into the substrates by wet chemical methods. The electrodes were metal-coated glass rods, soldered with indium along their entire length to metal films deposited in the grooves. While this approach was successful, and spectra in the mass range m/z = 0–50 were reported, there are several fundamental limitations that cannot easily be overcome.

The most serious problem is strong capacitive coupling across the insulating oxide layer at the rf drive frequency, an effect made worse by the large contact area between rods and substrate. This current leakage causes resistive heating of the silicon substrate, which melts the solder when scanning to higher than m/z = 50. There are also difficulties with the choice of material for the electrodes, since these must be compatible with the

soldering process but also have a thermal coefficient of expansion that approximately matches the substrate. Gold-coated glass rods were found to be a reasonably acceptable compromise, but these are far less convenient than stainless steel rods, which can be acquired from a number of suppliers. While a method of providing one-dimensional focusing was explored [25], a further limitation is that the design does not provide for any integrated components to efficiently couple ions into and out of the filter.

The quadrupole mass filter described and evaluated in the present paper is of an entirely different construction. The design is based on the use of bonded silicon on insulator (BSOI), a material consisting of two layers of silicon separated by an insulating layer of silicon oxide, which has become popular for both microelectronic and microengineering applications [26]. We have previously described details of the fabrication process, including mask design and process steps [16, 27]. BSOI can be structured using photolithography and deep reactive ion etching (DRIE) [28]. DRIE is a method of material removal based on the cyclic use of etching and sidewall passivation, which can form features that are many hundreds of micrometers deep at high rates and with excellent sidewall verticality [29]. An attractive feature is that multilevel features can be formed using stacked surface masks [30]. By combining these techniques, apertures, ion optical components, isolated electrical connections, and features designed to hold the rods can be created. One of the novel structures described in the present paper is a tubular tunnel electrode (referred to below simply as a tunnel) to couple ions into and out of the rod assembly. Similar structures, which are sometimes described as tube lenses, can be found in some conventional quadrupole mass spectrometers [24], but have not previously been integrated into a miniature filter. These tunnels must be electrically isolated, small enough to fit within the volume defined by the rods, and have thin walls so as to present a suitably large aperture. The ability to make such features is a distinct advantage of using silicon-based methods. Other microengineering techniques, such as the use of photoetched metal shim, are deceptively attractive as alternative methods of building miniature mass spectrometers. While reasonably precise and intricate components can be made cheaply using this technique, assembling anything other than the simplest structures can quickly become mired by the need to incorporate often bulky ceramic insulators, and the generally unavoidable use of nuts and bolts to hold the parts together. Accurate folding of miniature metal components to create more three-dimensional structures can also be challenging, and it is not clear how tunnels and rod supports of the size described here might be realized.

The purpose of this paper is to evaluate the performance of the filter in general, but with particular emphasis on the relative efficacy of simple apertures and tunnels for coupling ions into and out of the filter. Some details of the design and fabrication process are described first, as it is important to realize that there are limitations on the structures that can be produced. The electric fields present at the ends of the rod assembly have been modeled, and give some indication of how the filters might behave. However, the performance is primarily assessed by measuring the transmission as a function of resolution, and by demonstrating the mass range.

Design and Fabrication

An overview of a completed filter is presented in Figure 1a. The microengineered silicon structure has an overall size of 32 × 6 × 1 mm, and accommodates rods measuring (508 ± 5) μm in diameter and (30.650 ± 0.075) mm long. Rather than solder the rods into V-grooves, leaf springs are used to firmly push the rods at their ends against very thin, accurately etched support and alignment features. Any desired material can now be used for the rods, as no solder is used, and the design allows them to expand and contract independently of the rest of the structure. There is no capacitive coupling between the rods and the silicon, as these are directly connected. Although there is capacitive coupling between the grounded and rf carrying bonded silicon layers (separated by a thin-layer of oxide), the area of overlap may be reduced to an absolute minimum by selective etching.

A completed filter consists of an upper and a lower die, which are assembled to form a single, monolithic structure. Each die is made from a BSOI substrate, and incorporates all the mechanical and electrical features required to accommodate two rods. The starting BSOI wafer is prepared by the manufacturer with accurately specified layer thicknesses. The present application requires the so-called handle and device layers to be 400 and 80 μm thick, respectively, while the oxide layer between them is 2 to 4 μm thick. Photolithographic patterning of a photoresist, followed by deep reactive ion etching is used to create all the features in the substrate. The springs and vertical alignment features are etched into the thick handle layer whereas the electrical connections, horizontal alignment features, and ion optics are etched into the thinner device layer. As designed, the structure ideally accommodates rods of 500 μm diameter such that the inscribed radius, r_0, is 217 μm and the rod ratio is 1.15, which is close to the optimum theoretical [31] value of 1.147. In practice, the actual rod ratio was 1.16, as more readily available 508 μm diameter rods were used instead.

Some of the important structures in the design can be seen in the scanning electron microscopy (SEM) images shown in Figure 1b and c. There are vertical and horizontal features at the end of each rod, both of which are designed to provide the required alignment and mechanical support, while at the same time intruding as little as possible into the region between the rods. Note that there are four sets of support features in these images, and that each set is electrically isolated from the

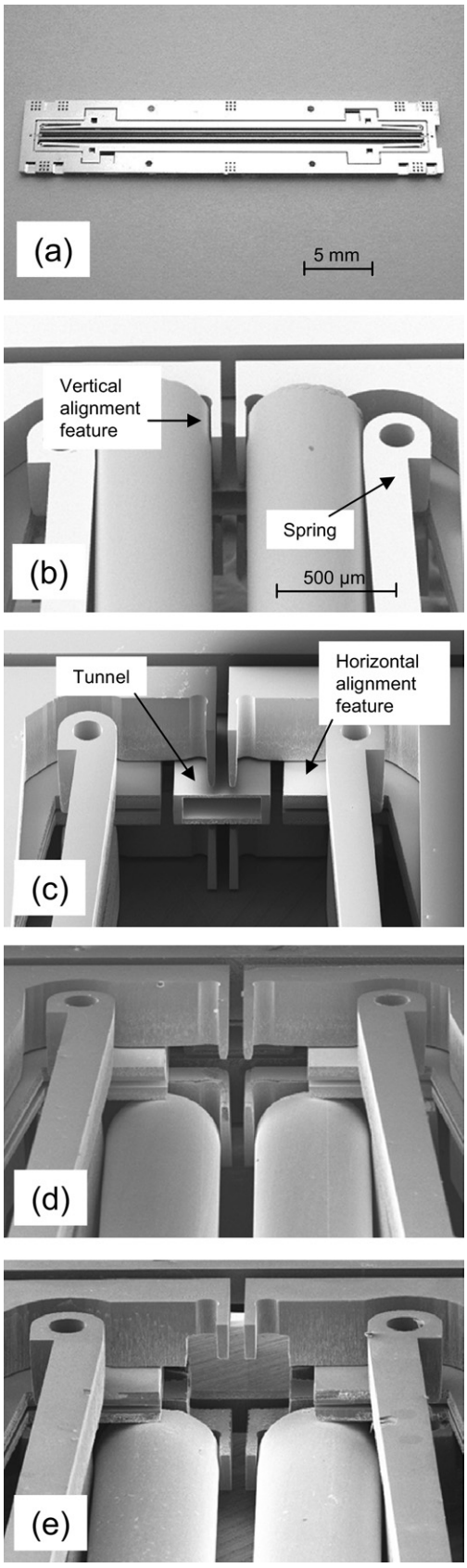

others. Although not obvious in Figure 1b, there is in fact a small gap between the end of each rod and the nearest silicon structure to allow for differential thermal expansion as well as small variations in the cut length of the rods. With the rods removed, the entrance tunnel can be seen at the center of the structure in Figure 1c. Its outer surfaces do not make contact with any of the four rods.

This arrangement is unlike conventional designs in which the ceramic support collars usually do not intrude into the field-defining region between the rods, and are sited well away from the ends. Not only do the horizontal and vertical support features extend into the quadrupole field, but they are also positioned at the very ends of the rod assembly. The horizontal supports are made just long enough to make tangential contact with the rods. However, the vertical supports are etched at the same time as the leaf springs, and consequently extend much further into the gaps between the rods. Note that the supports are in electrical contact with the rods and are, therefore, at the same potential.

We have assessed three design variants that are compatible with the chosen materials and processing techniques. The differences between these designs are visible in Figure 1c, d, and e. Figure 2 shows schematic representations of the same structures, together with SIMION 7.0 (Scientific Instrument Services, Ringoes, NJ) models of the electric potentials in the region of interest. In Figure 1c, the tunnel extends as far as the end of the horizontal and vertical supports, which is well into the region between the rods. The intention here is that the ions are shielded from the fields generated by the supports and are already within the confines of the rod assembly as they transit the fringing fields. The modeling shows that there is little field penetration into the tunnel (no more than 20–40 μm), and that the fields rise to their full values within 200 μm of the end of the tunnel. Similarly, Hunter and McIntosh [21] have found that there is only minimal penetration of the fields generated by the rods into an aperture placed in front of them. To maintain electrical isolation, the tunnel must not make contact with the rods. However, within this constraint, the tunnel cross-section is made as wide as possible to maximize transmission. Its height is dictated by the thickness of the device layer in which it is formed. The walls of the tunnel are made only 30 μm thick, again to maximize transmission. Also included in this design are two further lenses (referred to below as lens 1 and lens 2) before the entrance tunnel.

Figure 1. (**a**) Photograph and (**b**)–(**e**) scanning electron microscope (SEM) images of the microengineered quadrupole mass filter. Image (**b**) shows a completed filter with leaf springs pushing the rods against the vertical alignment features, while image (**c**) shows the same filter with the rods removed to reveal the horizontal alignment features and the entrance tunnel, which does not touch the rods. The small and large aperture designs are shown in images (**d**) and (**e**), respectively.

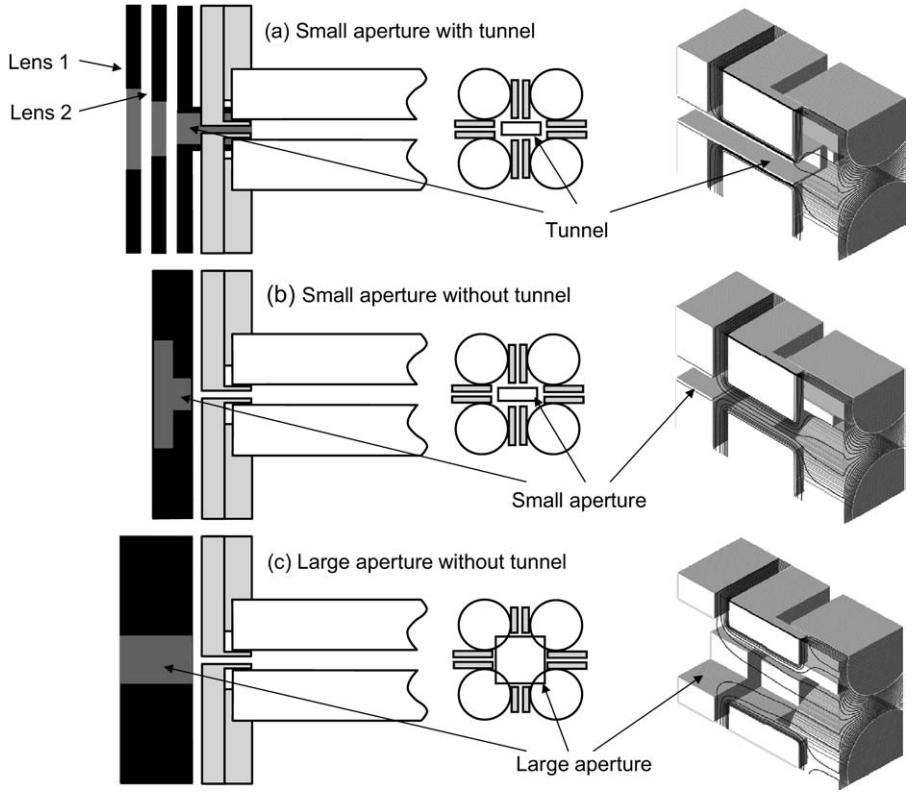

Figure 2. Schematic representation and SIMION models of the rod support structures, and the three types of coupling optics examined in this work. For clarity, the leaf springs are not shown. The views along the axis of the filter illustrate the size and position of the apertures with respect to the rods and their supports. Design (**a**) has lenses in addition to a tunnel at the input to the filter, but only a tunnel at the exit, while (**b**) and (**c**) have symmetric entrance and exit optics.

Like the tunnels, these are electrically isolated and may be biased. In the other two variants, there are apertures in the silicon frame, but no tunnels.

Figure 1d shows an arrangement that has an aperture with the same small cross-section as the tunnel variant. Ions passing through such an aperture are injected into a field that is expected to be unusually complex, asymmetric, and distorted. Indeed, the modeling shows that the quadrupole field is initially compressed in the vertical plane by the vertical supports. Further field distortions and asymmetry might result from the lack of axial alignment of the exposed rod ends (the rods are intentionally allowed to slip to accommodate any thermal expansion). Finally, the image in Figure 1e shows a departure from the original concept in which the aperture is not confined to the thin device layer and has been made large by etching through into the handle layer. Two potentially important consequences of doing this are that the ends of the rods are presented to the ions passing through the aperture, and that the vertical supports are cut back to half their original size during the same etch step. The modeling shows that the combined effect of a larger aperture and less intrusive vertical supports is a quadrupole field that is largely undistorted, and shows little evidence of the compression seen in Figure 2b.

Experimental

After assembly, every quadrupole mass filter was subjected to a series of measurements designed to track geometrical errors. The biggest errors are due to slip between the two die during assembly, variations in the thickness of the device layers, and small gaps between the two die. Within each die, the rod separation is controlled by the accuracy of the photolithography step, which is much less than 1 μm. A precision x-y stage fitted with Mitutoyo Digimatic Series 543 gauges (Mitutoyo America Corp. Aurora, IL) gauges was used to translate the filters with 1 μm resolution under a Leica optical microscope. The required dimensions were obtained by taking the difference between absolute position measurements when the microscope graticule was positioned on the relevant structural features. Using this technique, the thickness of the layers that separate the rods was found to vary from 159 to 167 μm, with an average value of 162 μm (the desired value is 160 μm), while the slip between the two die was found to vary from 0 to 8 μm, with an average value of 2 μm. In addition, one filter was inspected with a Wyko NT1100 optical profiler (Veeco Instruments Inc, Plainview, NY). This instrument showed that although there are some complex out-of-plane warping patterns, the overall

magnitude of these distortions do not exceed 10 μm along the entire length of the filter.

Following inspection, each filter was glued with an epoxy adhesive to a gold-plated PCB. Electrical connections were made from the PCB to bond pads on the filter using a KS 4523A wire-bonder. For the purposes of performance evaluation, the PCB was screwed to a stainless steel test assembly comprising of a commercially available electron impact ionization source, a channeltron detector (Detech 2120, Detector Technology Inc, Palmer, MA) in a separate enclosed chamber, and a CF35 flange with electrical feedthroughs. The test assembly was then fitted to a stainless steel vacuum chamber pumped by a 130 ls^{-1} turbo pump and equipped with a cold cathode pressure gauge. Although not discussed in this paper, a compact and portable mass spectrometer system based on the same miniature quadrupole mass filter chips has also been developed [32].

The ion source was similar in both size and design to the popular VG Anavac source. Given that such sources are intended for filters with 6 mm diameter rods, the ion beam produced has a much larger diameter than can be accommodated by the entrance aperture of the miniature filter. Typically, the radius of the focused ion beam exiting an ion source is arranged to be approximately half the inscribed radius of the filter. In the present case, the beam illuminates the whole of the entrance aperture and only 0.8% of the available ion current is sampled. For all experiments, the ion energy was 5 to 10 eV, which was set by applying 5 to 10 V to the cage with the pole bias at 0 V. The electron energy was 60 eV, and the emission current was 1 mA, the latter being controlled by a software PID loop.

The two out-of-phase rf waveforms required to drive the filters were supplied by a resonant amplifier driven by a 6 MHz waveform from an HP33120A signal generator. A 0 to 10 V dc command voltage was use to set the rf amplitude in a step-wise fashion during the course of a scan. One of the attractions of miniature quadrupole mass filters compared with larger instruments is the significantly lower rf and dc amplitudes needed to achieve a given mass range (these scale with the square of the rod radius). When the rod diameter is 0.5 mm and the drive frequency is 6 MHz, ion transmission at m/z = 400 requires an rf amplitude of 50 V (zero-to-peak). At the apex of the stable region in the stability diagram, the ratio of U, the dc amplitude, to V, the rf amplitude is close to 0.168 [13]. Hence, the maximum dc amplitude required is 8.3 V, which is conveniently supplied without further amplification by a standard PCI DAC card or similar.

Heat generation is an important consideration, as excessive temperatures might result in significant geometric distortion or structural failure. The ion source typically dissipated 2.5 to 4 W, which caused the temperature of the filter to rise by 14 to 23 °C, as measured by a thermocouple attached near the input. While scanning in the range m/z = 0–400, the power dissipated directly in the filter due to rf excitation was 0.3 to 1.2 W, and the additional temperature rise was 2 to 7 °C. A maximum total temperature rise of 30 °C causes the separation between the rods to increase by 0.02 μm, which is insignificant compared with other sources of geometric error. Although the rods expand in length by 13 μm more than the surrounding silicon, due to the higher thermal expansion coefficient of stainless steel, the leaf springs allow the structure to accommodate this differential expansion without distortion.

After pumping down to a base pressure of $\sim 1 \times 10^{-7}$ Torr, perfluorotributylamine (PFTBA) was admitted through a leak valve and allowed to flood the chamber to a pressure in the range of 2×10^{-6} to 5×10^{-6} Torr. To test the relative performance of each filter, spectra were recorded using a range of scan line gradients. The gradient of the scan line is equal to U/V, and determines the transmission and resolution of the filter. To ensure consistency, these sets of spectra were collected in an entirely automated manner using a LabView program (National Instruments Corp., Austin, TX), which controls the ion source emission, counts the pulses from the channeltron, and generates the three required dc voltages (one to control the rf amplitude, two to provide the $\pm$dc components of the drive waveform). Typically, 2000 data points were recorded for each m/z = 0–400 scan, with the counting period at each point set to 3 ms.

Ultimate resolution and mass range were examined further by recording spectra of the krypton isotopes and 2,6-diiodo-4-nitrophenol, respectively. Krypton gas was admitted through a leak valve as above, while 2,6-diiodo-4-nitrophenol (97%, Sigma-Aldrich, Poole, England), a solid at room temperature, was vaporized in an oven mounted inside the vacuum system. The mouth of the oven was positioned directly in front of an aperture in the ion source assembly that exposes the ionization region, as this compound condenses on any cold surface. A charge of ~100 mg lasted for several hours when the oven temperature was held at 120 °C.

Results and Discussion

A total of nine filters were characterized by recording spectra of PFTBA, as described above. Three had large apertures, two had small apertures, and the remainder had small apertures with tunnels. The spectra obtained using filters with small apertures and tunnels exhibited all the peaks expected for PFTBA in the m/z = 0–400 mass range. Filters with large apertures yielded spectra with a qualitatively similar distribution of peak heights, but the overall intensity was higher. The most striking result is the relatively poor performance, particularly at higher m/z, of the filters with small apertures but no tunnels. Representative spectra that illustrate the extent to which the presence of tunnels affects the performance are presented in Figure 3a and b. The data have been normalized such that the rf-only spectra recorded for the two filters have a maximum intensity of 1.0,

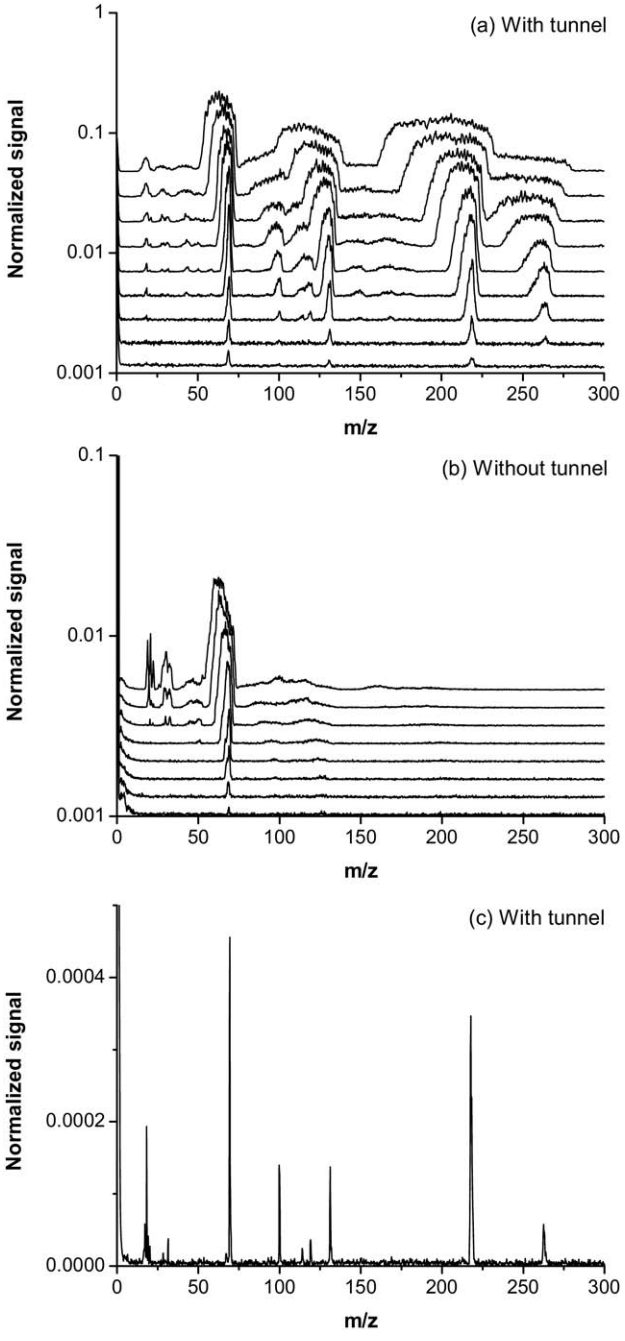

Figure 3. Sets of PFTBA spectra recorded using two filters, one with entrance and exit tunnels and the other with small apertures only, are shown in (**a**) and (**b**), respectively. Each set shows how the resolution and peak height distribution changes with U/V value, which increases from the top down. The spectra have been displaced vertically to aid presentation. Note that the intensities have been normalized by setting the transmission in rf-only mode to 1.0, and that a logarithmic scale has been used. The best spectrum recorded using a filter with tunnels, together with a modified scan line is plotted in (**c**).

although for clarity, these and other spectra in each set are not plotted. Linear scan lines with the dc offset set to zero were used to obtain both sets of data. In the absence of any other factors that might affect transmission or resolution, the peaks are expected to increase in both width and relative transmission with increasing mass. For analytical work, either a curved scan line, or a linear scan line with a dc offset would normally be used to give approximately uniform peak widths across the entire mass range.

Figure 3a shows that in the case of the filter with tunnels, $M/\Delta M$ is a constant, and peaks are present across the entire mass range. At high U/V ratios, the low mass peaks tend to extinguish first. When the tunnels are absent but the small aperture is retained, there is a substantial attenuation of the transmission that increases in severity with mass. In Figure 3b, peaks due to residual gas components and the m/z = 69 fragment of PFTBA are visible in the m/z = 0–100 mass range, but compared with Figure 3a, there is severe attenuation of the signal in the m/z = 100–300 mass range. In fact, the other PFTBA fragments are only just visible on close inspection when the scale is expanded. Figure 3c shows the best spectrum recorded using a filter with tunnels. In this case, a curved scan line has been used so as to decrease the resolution and increase the intensity of the low mass peaks. The m/z axis was calibrated by adjusting the scaling factor between commanded m/z value and rf amplitude until the 69 Da fragment appeared at m/z = 69. Even with this crude, single point calibration, data obtained using a number of filters showed that the 219 Da fragment appears at m/z = 218.9 ± 1.0.

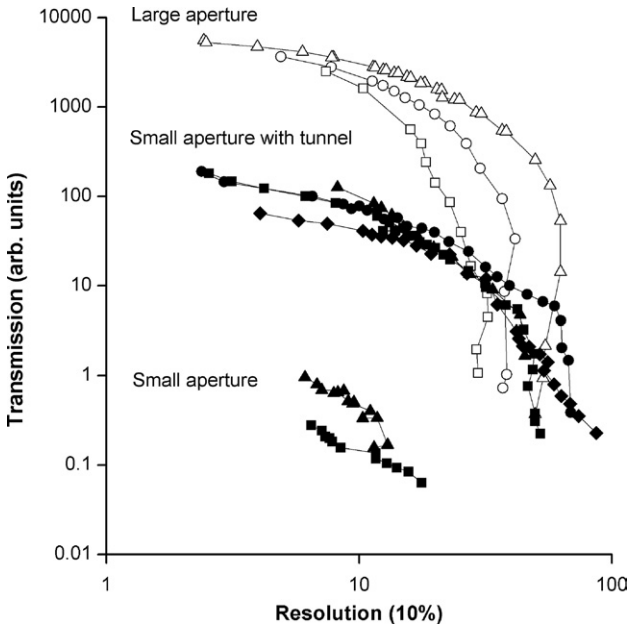

Figure 4. A plot of normalized transmission against resolution at m/z = 219 for the three design variants investigated. Lenses and tunnels were all grounded to compare only the geometrical aspects of the three variants. The ion energy was 10 eV. A total of nine filters were made, each of which yielded a transmission-resolution curve. The three groups of curves are labeled according to the filter design, and within each group, different symbols are used to distinguish the individual curves.

To better characterize the performance differences between the variants, the resolution was extracted for the m/z = 219 fragment of PFTBA and plotted against transmission. The results are presented in Figure 4. We have chosen to calculate the resolution using the full peak width measured at 10% of the peak height, rather than the more usual 50%, as the latter can sometimes be artificially small if the peaks are influenced by shoulders and splitting. The form of these transmission-resolution curves is typical of conventional quadrupole mass spectrometers. As the U/V ratio is increased, the resolution initially increases rapidly, with a relatively small decrease in transmission. However, at higher U/V ratios, there is a rapid drop in the transmission with little gain, or even a reduction in resolution [33].

The most notable feature of the data is the variation in transmission between the various designs. Filters with large apertures gave the best transmission, and an ultimate resolution in the range $M/\Delta M$ = 32 to 62. The resolution achieved with small apertures and tunnels is on average, slightly better and lies in the range $M/\Delta M$ = 45 to 87. However, this is at the expense of transmission, which drops by a factor of 30, although some of this can be recovered by suitable biasing of the tunnels, as described below. Removing the tunnels from the design to leave only the small apertures causes the transmission to drop by a further two to three orders of magnitude. Although not shown here, the resolution at m/z = 69 was also extracted and plotted against transmission. The effect of the tunnel is much less pronounced, as might be anticipated from Figure 3.

First, we consider filters with small apertures, and why tunnels influence the performance to such an extent. A significant observation is that the two designs, one with and the other without tunnels, yielded rf-only spectra of similar intensity. It is only as the resolution is increased that the difference in transmission of high mass ions becomes apparent. When the tunnel is absent, the severe attenuation of the signal as the dc component is added to the applied waveform suggests the involvement of what can loosely be described as fringing field defocusing.

The standard interpretation of fringing field defocusing [34] implies that the stability diagram has its usual form, and that the combined rf and dc fields rise smoothly from zero at some near-by grounded structure (normally the ion source exit aperture) to their full values just inside the rod assembly. The rf and dc fields experienced by the ions must, therefore, pass through the y-unstable region of the stability diagram as they evolve from the point at which they are zero, at the origin, to the set operating point in the stable region. While in the y-unstable region, ions are accelerated along the y axis, which may result in trajectories that are unfavorable for transmission. However, if the quadrupole is operated in rf-only mode, the field evolves entirely within the stable region and no fringing field defocusing is to be expected.

While this seems to be reflected by the results described above, the fact that the ions also transit a highly corrupted quadrupole field in the region between the rod supports must be considered as the primary contribution to defocusing. The trajectories of ions in a quadrupole field generated by round electrodes are described, to a good approximation, by the Mathieu equation, and the solutions to this equation determine the familiar regions of stable and unstable motion within the stability diagram. However, referring back to Figures 1d and 2b, it can be seen that the region between the aperture and the rods is dominated by the presence of the rod support features, which have a square section, asymmetric distribution, sharp edges, and also extend well into the gaps between the rods. The stable region of the stability diagram describing motion in this section is likely to be of a highly distorted shape, and is apparently not accessed as the dc component is increased. This interpretation is supported by the work of Hager [35], who showed that a poorly constructed quadrupole (which presumably also generated an imperfect field) was able to transmit ions in rf-only mode, but did not yield a resolved spectrum when a dc component was added to the waveform.

Although modeling [36] suggests a complicated relationship between the transmission probability and the number of rf cycles an ion spends within idealized fringing fields, the spectra in Figure 3b indicate that signal attenuation increases in severity with increasing mass. For a given ion energy, heavy ions travel more slowly than light ions. Hence, in this case, the longer an ion spends in the fringing fields, the less likely it is to be transmitted.

The presence of a tunnel seems to be very effective in by-passing the problematic region, although there will still be some fringing fields between the end of the tunnel and the surrounding rods. To further demonstrate how the presence of a tunnel minimizes the detrimental effects of fringing fields, a spectrum of 2,6-diiodo-4-nitrophenol, which has a molecular mass of 391 Da, is presented in Figure 5a. This compound was chosen since resonant stabilization of the molecular ion results in a prominent, high mass peak. It is clear from Figure 5a that not only is there a prominent peak at m/z = 391, but also that the distribution of peak intensities is in good agreement with the standard spectrum. This shows that the filter does not suffer from any significant mass discrimination effect that might be attributed to fringing fields.

The corrupted fields that dictate the coupling efficiency of filters with small apertures are much less significant in the case of filters with large apertures. While the difference in geometrical area of the apertures is ~3×, Figure 4 shows that the difference in transmission of the two filters without tunnels is 1000× to 10,000×. Comparing Figure 1d and e, the most obvious benefit of a large aperture is that the vertical support features are much further away from the center axis of the filter, and will consequently have a smaller influ-

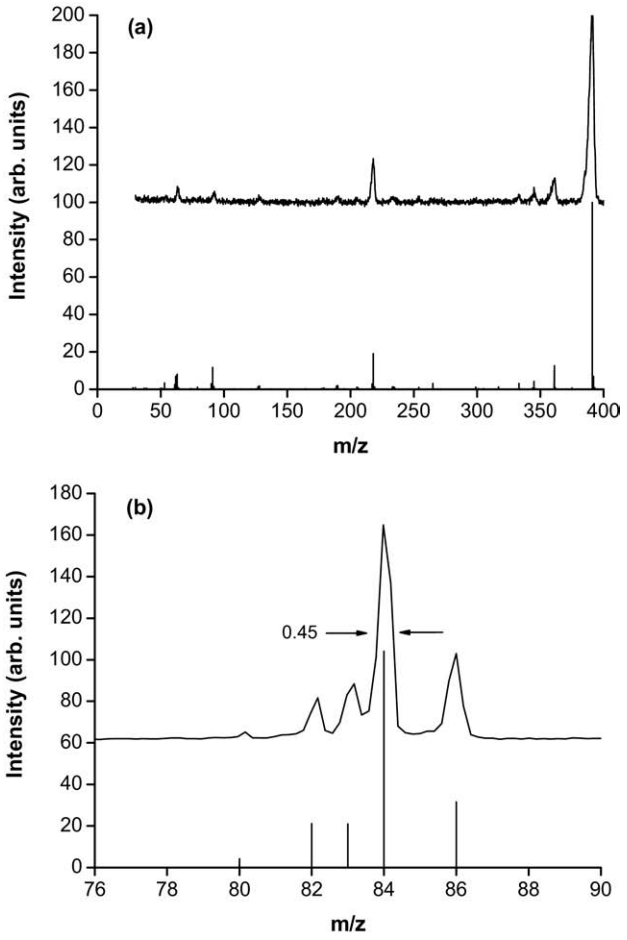

Figure 5. (**a**) Spectrum of 2,6-diiodo-4-nitrophenol demonstrating transmission of ions at m/z = 391. (**b**) Spectrum of the krypton isotopes showing peak widths of 0.45 mass units at 50% peak height, and 0.9 mass units at 10% peak height. For comparison, NIST standard spectra [37] are shown as vertical lines. Both spectra were obtained using a filter with tunnels.

ence on the field. In addition, the vertical and horizontal support features cause a symmetric distortion to the field as they all extend into the gaps between the rods by the same amount. This design has obvious similarities with more conventional quadrupole mass filters, and the fringing fields are expected to be determined by the interaction between the aperture, the exposed rod ends, and the entrance to the quadrupole field. However, it is not clear how the maximum resolution attainable could be improved. The large apertures are bigger than the inscribed circle and so do not restrict in any way the trajectories of ions entering or leaving the filter. The amplitude of oscillations within a quadrupole mass filter increases with the initial displacement of the ion from the central axis. It is desirable to restrict these oscillations to the central region of the filter where the effect of any field faults will be minimized. This is especially true for miniature filters, as microscopic roughness, dust particles, and rod distortions are of particular concern. Conventional analyzers typically incorporate an entrance aperture of approximately half the inscribed radius [13], and there is evidence that higher resolution can be achieved with even smaller apertures [38].

The ultimate resolution of any quadrupole mass filter increases with the square of the number of rf cycles the ions spend the filter, unless or until the resolution is limited by the accuracy of construction, or the purity of the rf waveform. When the rf frequency is 6 MHz and the axial ion energy is 10 eV, an ion with a mass of m/z = 219 spends ~60 cycles in the filter. According to Figure 6.2 in reference [13], this should result in an ultimate resolution of $M/\Delta M \approx 115$ at 10% peak height. As discussed earlier, the construction accuracy is of the order of several micrometers, or ~1%

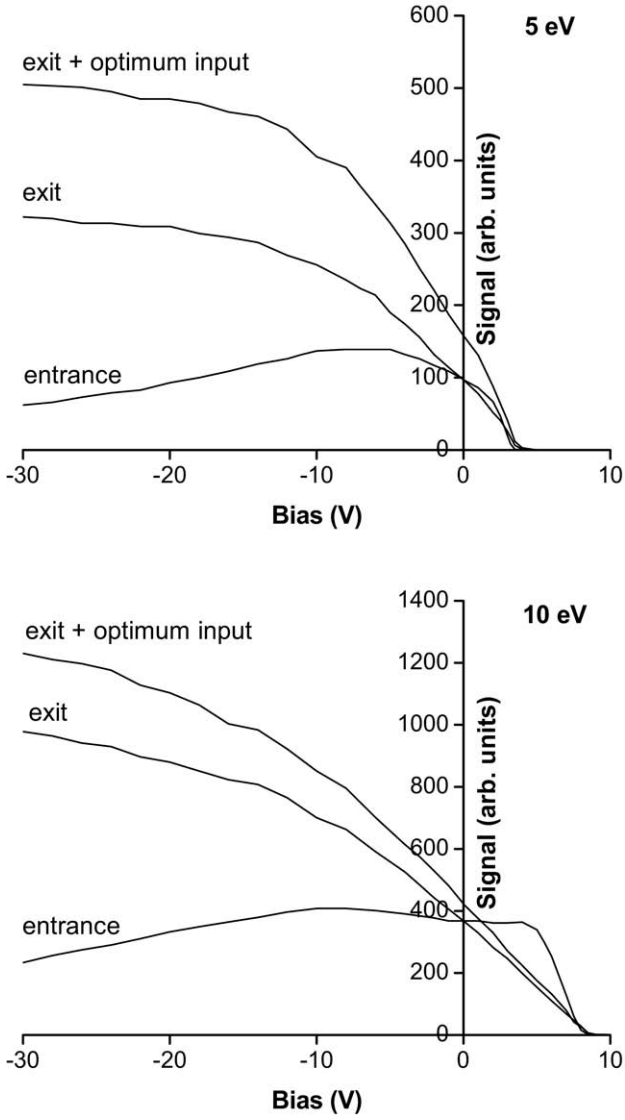

Figure 6. Response of the signal intensity in rf-only mode to biasing of the tunnels and associated lenses. The three sets of data plotted in each graph show the individual effect of biasing each tunnel with the other held at 0 V, and also the effect of exit tunnel bias with the entrance tunnel and lens 2 biases fixed at their optimum values. Transmission is enhanced by a factor of three at an ion energy of 10 eV, and five at an ion energy of 5 eV.

of the rod diameter. Hence, the ultimate resolution is expected to be limited by geometric errors to $M/\Delta M \approx 100$, according to Figure 6.3 in reference [13]. The best ultimate resolution in Figure 4 is $M/\Delta M = 87$, which is a little lower than might be expected if the number of rf cycles is limiting resolution, but is certainly consistent with the stated construction accuracy. Furthermore, there was no significant improvement in the observed resolution when the ion energy was reduced to 5 eV, which again suggests that the ultimate resolution is limited by the geometrical or electrical characteristics of the filter rather than the number of rf cycles.

A well-resolved spectrum of the krypton isotopes recorded using a filter with tunnels is shown in Figure 5b. The widths of the peaks are ~0.45 and 0.9 mass units at 50% and 10% peak height, respectively. This compares very favorably with the reported performance of three other miniature quadrupole filters, which were also able to resolve the krypton isotopes. An almost identical spectrum was obtained [2] using a miniature quadrupole mass spectrometer array developed for space applications. The array was constructed using 2 mm diameter rods that were held in position using machined ceramic jigs. As discussed earlier in connection with Table 1, the resolution that can be achieved is dictated by the accuracy of the construction technique and the degree of miniaturization attempted. Evidently, the design described in the present investigation allows the rod diameter to be reduced to 0.5 mm without degrading the performance in the $m/z = 0$–100 mass range. Slightly lower resolution was achieved with a filter constructed using ceramic spacers and ideal hyperbolic electrodes [3], which were positioned to give an inscribed radius of 0.33 mm (about 50% bigger than the inscribed radius defined by 0.5 mm diameter rods). An array described by Boumsellek and Ferran [4, 14] also yielded slightly lower resolution at 50% peak height, but very similar base line separation. This filter was constructed using 1 mm diameter rods that were bonded to glass supports using an accurate glass-to-metal sealing technique.

As indicated earlier, any ion optical components included in the device layer can be individually biased for best performance. The data in Figure 4 were obtained with the bias on all lenses and tunnels set to zero, to compare only the geometrical aspects of the various designs. In a previous paper [16], the focusing action of lens 2 with lens 1 and the tunnels held at 0 V was described. This Einzel lens arrangement resulted in a distinct maximum at +8 V when the ion energy was 10 eV. Subsequent investigations have revealed that this enhancement is only significant when the ion beam exiting the ion source is misaligned with respect to the axis of the filter. The Einzel lens acts to focus the off-axis ion beam into the rod assembly. However, when the ion beam is better aligned and evenly illuminates the entrance aperture, no such correction is required, and a plot of signal intensity against lens 2 bias exhibits only weak maxima.

However, an alternative mode of operation is possible when tunnels are present. Figure 6 shows how a signal enhancement of 3× and 5× can be achieved by appropriate biasing of the tunnels when the ion energy is 10 and 5 eV, respectively. The effect of each tunnel was examined individually by holding the other tunnel and the lenses at 0 V. An increase in the count rate was observed at negative biases, particularly so in the case of the exit tunnel. To find the maximum possible signal enhancement, the bias on the entrance tunnel was first set to its optimum value. Although its effect is relatively small, the bias on lens 2 bias was then adjusted for maximum signal. Finally, as shown in Figure 6, the signal was recorded as the exit tunnel bias was varied. Similar sets of data have been obtained for a number of filters of the same design and at various U/V values. There is some degree of variability, which is likely to be due to the surface finish, misalignment, and other processing related effects, as well as deposition of dielectric material during use (particularly on the entrance optics). Signal enhancements of up to 15× have been recorded, although this is not considered representative of the general performance. Note that the energy of the ions within the quadrupole field is not changed by the tunnel bias, as this is defined by the rod bias. By applying a positive voltage equal to the ion source cage potential to either tunnel, the transmission of ions can be completely attenuated. This feature may be of use in applications requiring ion gating, especially since the low capacitances involved allow this to be done rapidly. Dobson and Enke [39] have used tubular tunnel electrodes in a similar manner to focus and contain ions in a very short linear ion trap.

Conclusions

At low resolution, the best transmission is achieved using filters in which the rod supports and surrounding frame are cut back to leave the largest aperture that can be accommodated by the substrate. This design is somewhat unsatisfactory in that ions can enter the filter far from the central axis of the field. The lack of axial alignment of the rods and the rough finish of their end faces are also factors that may limit the performance. Unfortunately, when the depth of the etch that defines the entrance aperture is restricted to the device layer, the vertical rod supports are not cut back. These generate highly distorted fields at the entrance to the filter, which result in a significant reduction in transmission of higher mass ions. However, a tunnel that injects ions directly into the field between the rods can be incorporated into the structure with little extra effort, and uniform transmission of ions across the whole mass range is restored. Some further gains in transmission are possible when the tunnels are biased.

We conclude that the design incorporating a tunnel is the most suitable candidate for further development. The best resolution achieved is sufficient for simple analytical work. Apparently, the ultimate resolution is

limited by geometrical errors or the electrical characteristics of the filter, rather than the number of rf cycles experienced by the ions. The performance could be enhanced, therefore, by improvements in the accuracy of the die-to-die bonding technique, the straightness and diameter tolerance of the rods, and the electrical characteristics of the processed BSOI substrate.

To an extent, the coupling of ions from an external ion source into the quadrupole field has been made difficult by the chosen design philosophy. Unusually, perhaps even uniquely, the entrance to the filter is dominated by structures required to hold the rods and provide electrical connections. This approach was taken because it addresses difficulties that arise in designs relying on solder to hold the rods in place. Fortunately, the use of a multilayer substrate and planar silicon processing techniques allows very small yet evidently critical structures, such as the tunnels, to be integrated into the filter.

Acknowledgments

The authors are indebted to M.-A. Schwab, Alan Finlay, Andrew Malcolm, Dr. R. Moseley, and Dr. N. Dash for their valuable contributions to this work.

References

1. Badman, E. R.; Cooks, R. G. Miniature Mass Analyzers. *J. Mass Spectrom.* **2000,** *35,* 659–671.
2. Orient, O. J.; Chutjian, A.; Garkanian, V. Miniature High-resolution Quadrupole Mass-spectrometer Array. *Rev. Sci. Instrum.* **1997,** *68,* 1392–1397.
3. Holkeboer, D. H.; Karandy, T. L.; Currier, F. C.; Frees, L. C.; Ellefson, R. E. Miniature Quadrupole Residual Gas Analyzer for Process Monitoring at milliTorr Pressures. *J. Vac. Sci. Technol.* **1998,** *A16,* 1157–1162.
4. Ferran R. J.; Boumsellek S. High Pressure Effects in Miniature Arrays of Quadrupole Analyzers for Residual Gas Analysis from 10^{-9} to 10^{-2} Torr. *J. Vac. Sci. Technol.* **1996,** *A14,* 1258–1265.
5. Velasquez-Garcia, L. F.; Akinwande, A. I. An Out-of-plane MEMS Quadrupole for a Portable Mass Spectrometer. *Proceedings of the Transducers Eurosensors conference*; Lyon, France, June 2007; p. 2315–2320.
6. Taylor, S.; Tindall, R.; Syms, R. R. A. Silicon Based Quadrupole Mass Spectrometry Using Microelectromechanical Systems. *J. Vac. Sci. Technol.* **2001,** *B19,* 557–562.
7. Brewer, R. G.; Devoe R. G.; Kallenbach R. Planar Ion Microtraps. *Phys. Rev.* **1992,** *A46,* R6781–R6784.
8. Wells, J. M.; Badman E. R.; Cooks R. G. A Quadrupole Ion Trap with Cylindrical Geometry Operated in the Mass-Selective Instability Mode. *Anal. Chem.* **1998,** *70,* 438–444.
9. Badman, E. R.; Johnson, R. C.; Plass, W. R.; Cooks, R. G. A Miniature Cylindrical Quadrupole Ion Trap: Simulation and Experiment. *Anal. Chem.* **1998,** *70,* 4896–4901.
10. Petzold, G.; Siebert, P.; Muller, J. A Micromachined Electron Beam Ion Source. *Sensors Actuators* **2000,** *B67,* 101–111.
11. Wilfert, S.; Edelmann, C. Miniaturized Vacuum Gauges. *J. Vac. Sci. Tech.* **2004,** *A* 22, 309–320.
12. Kline-Schoder, R. J.; Sorensen, P. H. Miniature High Vacuum Pump for Mass Analytical Instruments. *Proceedings of the American Vacuum Society 54th International Symposium*; October, 2007, Seattle, Washington, USA.
13. Dawson, P. H. Quadrupole Mass Spectrometry and Its Applications; Elsevier Scientific: Amsterdam, 1976.
14. Boumsellek, S.; Ferran, R. J. Trade-Offs in Miniature Quadrupole Designs. *J. Am. Soc. Mass Spectrom.* **2001,** *12,* 633–640.
15. Wiberg, D.; Myung, N. V.; Eyre, B.; Shcheglov, K.; Orient, O.; Moore, E.; Munz, P. LIGA Fabricated Two-dimensional Quadrupole Array and Scroll Pump for Miniature Gas Chromatograph/Mass Spectrometer. *SPIE Proc.* **2003,** *4878,* 8–13.
16. Geear, M.; Syms, R. R. A.; Wright, S.; Holmes, A. S. Monolithic MEMS Quadrupole Mass Spectrometers by Deep Silicon Etching. *J. Micromech. Sys.* **2005,** *14,* 1156–1166.
17. Syms, R. R. A.; Tate, T. J.; Ahmad, M. M.; Taylor, S. Design of a Microengineered Quadrupole Electrostatic Lens. *IEEE Trans. Electron Devices* **1998**, *TED-45,* 2304–2311.
18. Kornienko, O.; Reilly, P. T. A.; Whitten, W. B.; Ramsey, J. M. Micro Ion Trap Mass Spectrometry. *Rapid Commun. Mass Spectrom.* **1999,** *13,* 50–53.
19. Pau, S.; Pai, C. S.; Low, Y. L.; Moxom, J.; Reilly, P. T. A.; Whitten, W. B.; Ramsey, J. M. Microfabricated Quadrupole Ion Trap for Mass Spectrometer Applications. *Phys. Rev. Lett.* **2006,** *96,* 120801.
20. Dawson, P. H. Fringing Fields in the Quadrupole Mass Filter. *Int. J. Mass Spectrom. Ion Phys.* **1971,** *6,* 33–44.
21. Hunter K. L.; McIntosh, B. J. An Improved Model of the Fringing Fields of a Quadrupole Mass Filter. *Int. J. Mass Spectrom. Ion Processes* **1989,** *87,* 157–164.
22. Blaum, K.; Geppert, C.; Müller, P.; Nörtershäuser, W.; Otten, E. W.; Schmitt, A.; Trautmann, N.; Wendt, K.; Bradshaw, B. A. Properties and Performance of a Quadrupole Mass Filter used for Resonance Ionization Mass Spectrometry. *Int. J. Mass Spectrom.* **1998,** *181,* 67.
23. Barnett, E. F.; Tandler, W. S. W.; Turner, W. R. Quadrupole Mass Filter with Fringing-Field Penetrating Structure. *U.S.A. Patent no.* 3560734.
24. Brubaker, W. M.; Tuul, J. Performance Studies of a Quadrupole Mass Filter. *Rev. Sci. Instrum.* **1964,** *35,* 1007–10.
25. Syms, R. R. A.; Michelutti, L.; Ahmad, M. M. Two-Dimensional Microfabricated Electrostatic Einzel Lens. *Sensors Actuators A* **2003,** *107,* 285.
26. Benitez, A.; Esteve, J.; Bausells, J. Bulk Silicon Microelectromechanical Devices Fabricated from Commercial Bonded and Etched-Back Silicon-on-Insulator Substrates. *Sensors Actuators* **1995,** *A50,* 99–103.
27. Syms, R. R. A. Monolithic Microengineered Mass Spectrometer. European patent no. EP1540697, U.S.A. Patent no. 7208729.
28. Klaassen, E. H.; Petersen, K.; Noworolski, J. M.; Logan, J.; Maluf, N. I.; Brown, J.; Storment, C.; McCulley, W.; Kovacs, T. A. Silicon Fusion Bonding and Deep Reactive Ion Etching: A New Technology for Microstructures. *Sensors Actuators* **1996,** *A52,* 132–139.
29. Hynes, A. M.; Ashraf, H.; Bhardwaj, J. K.; Hopkins, J.; Johnston, I.; Shepherd, J. N. Recent Advances in Silicon Etching for MEMS Using the ASE™ Process. *Sensors Actuators* **1999,** *74,* 13–17.
30. Mita, Y.; Tixier, A.; Oshima, S.; Mita, M.; Gouy, J.-P.; Fujita, H. A Silicon Shadow Mask with Unlimited Patterns and a Mechanical Alignment Structure by Al-Delay Masking Process. *Trans. JIEE* **2000,** *120–E,* 357–362.
31. Denison, D. R. Operating Parameters of a Quadrupole in a Grounded Cylindrical Housing. *J. Vac. Sci. Technol.* **1971,** *2,* 266–269.
32. Finlay, A.; Syms, R. R. A.; Wright, S.; Malcolm, A. Microsaic Ionchip: The First Commercially Available Mass Spectrometer Chip. *Proceedings of the 57th Annual Pittsburgh Conference on Analytical Chemistry and Applied Spectroscopy*; Pittcon 06, Orlando, FL, March 2006; p. 681.
33. Ma, F. M.; Taylor, S. Simulation of the Ion Trajectories through the Mass Filter of a Quadrupole Mass Spectrometer. *IEE Proc A* **1996,** *143,* 71–76.
34. Brubaker, W. In *Advances in Mass Spectrometry*, Vol. IV, Kendrick, E., Ed.; Institute of Petroleum: London, 1968; p. 293.
35. Hager, J. W. Performance Optimization and Fringing Field Modifications of a 24-mm Long rf-only Quadrupole Mass Spectrometer. *Rapid Commun. Mass Spectrom.* **1999,** *13,* 740–748.
36. Dawson, P. H. The Acceptance of the Quadrupole Mass Filter. *Int. J. Mass Spectrom. Ion Phys.* **1975,** *17,* 423–445.
37. NIST Mass Spectral Library, Gaithersburg, MD.
38. Brubaker, W. M.; Tuul, J. Performance Studies of a Quadrupole Mass Filter. *Rev. Sci. Instrum.* **1964,** *35,* 1007–1010.
39. Dobson, G. S.; Enke, C. G. Axial Ion Focusing in a Miniature Linear Ion Trap. *Anal. Chem.* **2007,** *79,* 3779–3785.